Original Research

Measurement of Signal-to-Noise Ratios in MR Images: Influence of Multichannel Coils, Parallel Imaging, and Reconstruction Filters

Olaf Dietrich, PhD,[1]* José G. Raya, MSc,[1] Scott B. Reeder, MD, PhD,[1,2] Maximilian F. Reiser, MD,[1] and Stefan O. Schoenberg, MD[1]

Purpose: To evaluate the validity of different approaches to determine the signal-to-noise ratio (SNR) in MRI experiments with multi-element surface coils, parallel imaging, and different reconstruction filters.

Materials and Methods: Four different approaches of SNR calculation were compared in phantom measurements and in vivo based on: 1) the pixel-by-pixel standard deviation (SD) in multiple repeated acquisitions; 2) the signal statistics in a difference image; and 3) and 4) the statistics in two separate regions of a single image employing either the mean value or the SD of background noise. Different receiver coil systems (with one and eight channels), acquisitions with and without parallel imaging, and five different reconstruction filters were compared.

Results: Averaged over all phantom measurements, the deviations from the reference value provided by the multiple-acquisitions method are 2.7% (SD 1.6%) for the difference method, 37.7% (25.9%) for the evaluation of the mean value of background noise, and 34.0% (38.1%) for the evaluation of the SD of background noise.

Conclusion: The conventionally determined SNR based on separate signal and noise regions in a single image will in general not agree with the true SNR measured in images after the application of certain reconstruction filters, multichannel reconstruction, or parallel imaging.

Key Words: MR imaging; image analysis; signal-to-noise ratio; parallel imaging; postprocessing filters
J. Magn. Reson. Imaging 2007;26:375–385.
© 2007 Wiley-Liss, Inc.

THE SIGNAL-TO-NOISE RATIO (SNR) is an important quantity used to describe the performance of a magnetic resonance imaging (MRI) system, and is frequently used for image evaluation, measurement of contrast enhancement, pulse sequence and radiofrequency (RF) coil comparison, and quality assurance. Several methods to determine the SNR of MR images have been described. The most commonly used technique is based on the signal statistics in two separate regions of interest (ROIs) from a single image: one in the tissue of interest to determine the signal intensity, and one in the image background to measure the noise intensity (1,2). There are two important preconditions for SNR measurements based on this "two-region" approach: a spatially homogeneous distribution of noise over the whole image is required, and the statistical intensity distribution of the noise should be known so that the noise properties measured in a background area can be used to deduce the noise distribution overlaying the anatomic structures in the foreground. These assumptions have been valid for many MR images in past years, particularly for those acquired by spin-warp imaging (image reconstruction by 2D or 3D Fourier transform) with a standard single-channel volume quadrature coil followed by a magnitude reconstruction.

However, the use of newly developed phased-array surface coil systems and new reconstruction techniques, such as parallel imaging (3,4), can influence both the statistical and the spatial distribution of noise. For instance, the noise distribution in parallel imaging is described by the spatially varying geometry factor (g-factor) and depends on parameters such as the coil geometry, phase-encoding direction, and acceleration factor (4,5). In this case the determination of the noise intensity using a background ROI may lead to inaccurate results and thus to over- or underestimation of SNR. Similarly, the sum-of-squares (SoS) reconstruction for data from phased-array coils (6) changes the statistical distribution of background noise (7), and even the application of reconstruction filters can influence the spatial distribution of noise. These effects are of particular importance if the SNR is used to compare methods that differently influence the noise distribu-

tion, such as MRI using nonaccelerated vs. parallel-imaging methods. Nevertheless, in many recently published studies evaluating parallel imaging (8–18), SNR calculations were performed using the two-region approach despite the questionable validity of this method.

The purpose of this study was to evaluate the validity of the two-region approach in comparison with two alternative techniques in MRI experiments with multi-element surface coils and parallel-imaging techniques, and after the application of different reconstruction filters, i.e., in situations where an altered probability distribution and an inhomogeneous spatial distribution of background noise must be expected.

MATERIALS AND METHODS

Phantom experiments were performed on a 1.5-T whole-body MRI system (Magnetom Sonata; Siemens Medical Solutions, Erlangen, Germany) to compare four different methods of SNR measurements in acquisitions with three different pulse sequences, two receiver coil systems, and different reconstruction techniques as described below. To demonstrate the validity of our results in vivo, we also performed SNR measurements in a volunteer who provided written informed consent to participate in the study, which had local institutional review board approval.

Methods of SNR Measurement

Several methods to measure the SNR have been described. They can be differentiated into methods based on a single image, on a pair of images, or on a series of many images. SNR measurements based on two ROIs in a single image (one in the tissue of interest, and one in the image background, i.e., in air, outside the imaged object) can be subdivided into methods using the standard deviation (SD) of the background intensity and those using the mean value of the background intensity (1,2). We refer to these two-region methods as SNR_{stdv} and SNR_{mean}, respectively. With the appropriate conversion factors derived from the noise statistics, both methods yield identical results.

An alternative method of SNR determination is the "difference method," which is based on the evaluation of a difference image of two repeated (identical) acquisitions (19–23). We refer to this approach as SNR_{diff}. A further method based on two images is suggested in the NEMA standard MS 1-2001 (21) and is therefore referred to as SNR_{NEMA}. It is based on the acquisition of a normal magnitude image and a pure noise image. Recently, Kellman and McVeigh (23) suggested image reconstruction in SNR units. This method (referred to as SNR_{units}) is based on noise measurements in additional noise scans and yields images with pixel intensities directly presenting SNR estimates. Finally, one can employ the most commonly used definition of the SNR of a single image voxel as the ratio of the mean value and the SD of the signal intensity time course of the voxel in repeated "identical" acquisitions (5,7,22–25). According to this definition, the noise of a single voxel is described by the stochastic variation of its signal intensity in repeated acquisitions. We refer to this approach as

SNR_{mult}. Mathematical descriptions of these methods of SNR determination are presented in Appendix A.

Since SNR_{mult} has the weakest requirements on the statistical and spatial distribution of noise, the validity of other methods can be evaluated by comparing their results with SNR_{mult} as the standard of reference. In this study, SNR_{NEMA} and SNR_{units} were not evaluated because of the technical difficulties involved. SNR_{NEMA} is based on the acquisition and reconstruction of a pure noise image. This cannot be done without modifying the applied pulse sequences as well as the image-reconstruction algorithms, and is especially demanding when using autocalibrating parallel-imaging techniques, since noise data must be reconstructed using the same coil sensitivity profiles that were acquired for the image itself. Similarly, SNR_{units} requires pulse sequence modifications to acquire the additional noise scans and a completely new reconstruction algorithm.

MRI Acquisition Techniques: RF Coils and Parallel Imaging

Measurements were performed with a standard single-channel (1CH) quadrature head coil and a dedicated eight-channel (8CH) surface coil array for parallel imaging consisting of 12 coil elements (six posterior and six anterior). Eight of these 12 elements were combined in pairs of two, such that together with the remaining four elements the coil system matched the eight receiver channels of the MRI system. With the 1CH coil, only nonaccelerated acquisitions without parallel imaging were performed. With the 8CH coil, phantom images were acquired with and without parallel imaging. Parallel-imaging data were reconstructed using the generalized autocalibrating partially parallel acquisition (GRAPPA) algorithm (26) and a modified sensitivity-encoding (mSENSE) algorithm (27). For parallel imaging, the acceleration factor was 2, and the number of reference lines used for autocalibration and the calculation of coil sensitivity profiles was 24.

MRI Reconstruction Techniques: Reconstruction Filters

For all four acquisition techniques, we compared image reconstruction without any additional filtering and with four different reconstruction filters: a Hanning filter, a large-field-of-view (large-FOV) correction filter, an intensity-normalization filter, and an elliptical low-pass filter. The Hanning filter gives higher weighting to central k-space data and lower weighting to peripheral k-space data. This filter can increase the SNR and reduce edge ringing; however, the spatial image resolution is also decreased to a certain degree. The large-FOV compensation filter is used to correct geometric distortions, such as "pin-cushion" distortions at the edges of the FOV. The intensity-normalization filter is used to compensate for a spatially varying intensity distribution caused by inhomogeneous coil profiles (typically applied for surface coil systems). The elliptical low-pass filter sets the corners of the k-space to zero, and thus can improve the SNR without substantially decreasing spatial resolution.

MRI Pulse Sequences: Imaging Parameters

Three different pulse sequences were used in this study: a single-shot spin-echo echo-planar imaging (EPI) sequence, a spin-echo-based single-shot half-Fourier-acquired "rapid acquisition with relaxation enhancement" (hF-RARE) sequence, and a fully gradient-balanced steady-state free-precession (SSFP) sequence. With all three sequences we acquired one slice in transverse orientation with a slice thickness of 8 mm and in the phase-encoding direction from left to right. The EPI sequence was applied with a matrix of 192×192, TR of 1000 ms, TE of 100 ms, and a bandwidth of 1132 Hz/pixel acquiring 6/8 (75%) of the k-space in the phase-encoding direction (partial-Fourier acquisition). The hF-RARE sequence was applied with a matrix of 256×256, TR of 1000 ms, TE of 75 ms, and a bandwidth of 488 Hz/pixel, acquiring 4/8 (50%) of k-space in the phase-encoding direction. The SSFP sequence was applied with a matrix of 256×256, TR of 4.3 ms, TE of 2.15 ms, and a bandwidth of 930 Hz/pixel, acquiring the full k-space in the phase-encoding direction.

Phantom Measurements

With the three pulse sequences described above, we acquired images of a cylindrical liquid phantom (T1 = 280 ms, T2 = 240 ms) with a square FOV of 300×300 mm^2 and 100 repetitions. These measurements were performed with the four acquisition techniques (1CH nonaccelerated, 8CH nonaccelerated, 8CH GRAPPA, and 8CH mSENSE) and the five reconstruction techniques (no filter, Hanning filter, large-FOV compensation, intensity normalization, and elliptical filter) described above. This resulted in 20 experiments for each of the three evaluated sequences, and thus a total number of 60 phantom experiments.

In all of these 60 experiments, we measured the SNR using four different methods: SNR_{mult}, SNR_{diff}, SNR_{mean}, and SNR_{stdv}. SNR_{mult} was calculated from repetitions 6–100 to avoid any initial non-steady-state images, SNR_{diff} was calculated from repetitions 6 and 7, and SNR_{mean} and SNR_{stdv} were calculated from repetition 6. A linear intensity correction was applied to repetitions 6–100 before calculating SNR_{mult} to compensate for any remaining intensity drift during the acquisition. A square ROI (ROI area $32 \times 32 = 1024$ pixels) positioned centrally in the phantom was used for SNR calculations with the methods SNR_{mult} and SNR_{diff}, and to calculate the mean signal intensity for SNR_{mean} and SNR_{stdv}. An additional rectangular ROI (ROI area $64 \times 16 = 1024$ pixels) positioned outside the phantom (close to the image edge in the readout direction) was used to calculate the noise intensity for SNR_{mean} and SNR_{stdv}. Finally, based on the pixel-by-pixel SD determined for SNR_{mult}, noise maps displaying this SD as a grayscale image were calculated.

In Vivo Measurements

In vivo measurements were performed in a healthy volunteer (male, 33 years old) with the SSFP sequence described above. The same acquisition parameters were used, except for a larger FOV of 400×400 mm^2 and only 10 repetitions to allow breath-hold imaging. The acquired slice was positioned over the upper abdomen in transverse orientation. We used the conventional body coil for acquisitions with one receiver channel, and the 12-element phased-array coil described above for acquisitions with eight receiver channels. By applying the same reconstruction filters as for the phantom measurements, a total number of 20 experiments were performed. In all experiments, we measured the SNR with three different methods: SNR_{diff} was calculated from repetitions 9 and 10, and SNR_{mean} and SNR_{stdv} were calculated from repetition 10. The last two repetitions of each acquisition were chosen to avoid any initial non-steady-state effects. A square ROI (ROI area $20 \times 20 = 400$ pixels) positioned in the liver parenchyma was used for SNR calculations with the method SNR_{diff}, and to calculate the mean signal intensity for SNR_{mean} and SNR_{stdv}. An additional rectangular ROI (ROI area $40 \times 10 = 400$ pixels) positioned outside the abdomen (close to the image edge in the readout direction) was used to calculate the noise intensity for SNR_{mean} and SNR_{stdv}.

Since the acquisition of a sufficiently large number of repetitions for SNR_{mult} is not feasible in breath-hold duration, we did not measure SNR_{mult} in vivo; instead, we used SNR_{diff} as the standard of reference and compared the calculated SNR values with SNR_{diff} to assess the precision of the different methods.

Data Evaluation

All SNR measurements were based on the magnitude image data provided by the standard image reconstruction of the MRI system. We used Bland-Altman plots (28,29) to compare the calculated SNRs with the standard of reference (SNR_{mult} in the phantom measurements and SNR_{diff} in the volunteer measurements) and to assess the precision of the different methods. The ratio of the range of the 95% confidence interval (CI) and the average SNR was calculated as a scalar measure that describes the quality of the method of SNR measurement. In addition, we calculated the relative deviations from the standard of reference, i.e., $|SNR_{diff/mean/stdv} - SNR_{mult}| / SNR_{mult}$ for the phantom experiments, and $|SNR_{mean/stdv} - SNR_{diff}| / SNR_{diff}$ for the measurements in vivo. In general, deviations of less than 10% were considered as acceptable. Finally, we calculated different SNR ratios comparing the 8CH acquisitions without parallel imaging to the 1CH acquisitions, comparing the 8CH acquisition with GRAPPA or mSENSE to the 8CH acquisitions without parallel imaging, and comparing the acquisitions with each of the four applied reconstruction filters to the acquisitions without filtering. These ratios were calculated for all methods of SNR measurements. For the phantom experiments, we compared these SNR ratios to the results calculated from the standard of reference, SNR_{mult}, using the Wilcoxon matched-pairs signed-ranks test. In vivo, the number of experiments was too low to allow statistical evaluation.

RESULTS

Phantom Measurements

Evaluating all 60 phantom measurements, the relative deviations determined for SNR_{diff} range from 0% to 7.6%, and thus are always lower than 10%. The relative deviations of SNR_{mean} range from 0.3% to 100.4%, and the relative deviations of SNR_{stdv} range from 0% to 139.9%. Averaged over all sequences and all measurements, the deviations from SNR_{mult} are 2.7% ($\pm$SD 1.6%) for SNR_{diff}, 37.7% ($\pm$25.9%) for SNR_{mean}, and 34.0% ($\pm$38.1%) for SNR_{stdv}.

In 53 of all 60 measurements, the deviation of SNR_{mean} was greater than 10%. The seven measurements with deviations lower than 10% were all performed with the 1CH head coil without parallel imaging. One of these seven measurements was acquired with the hF-RARE pulse sequence (and the intensity normalization filter). The other six were acquired with the SSFP or EPI pulse sequences and no filter, the Hanning filter, or the elliptical filter.

In 37 of all 60 measurements, the deviation of SNR_{stdv} was greater than 10%. These included all measurements with the large-FOV filter and most of the measurements with the intensity-normalization filter (except in combination with the 8CH coil and nonaccelerated imaging). Of the 23 measurements with deviations lower than 10%, 21 were performed without parallel imaging and only two were obtained with mSENSE (and the SSFP pulse sequence combined with the Hanning or intensity-normalization filter).

The deviations from SNR_{mult} are presented as Bland-Altman plots for the three different methods in Fig. 1, which shows 95%-CIs between –9.7 and 7.0 for SNR_{diff}, between –116 and 114 for SNR_{mean}, and between –97 and 56 for SNR_{stdv}. The ratio of the range of the 95%-CI and the average SNR is 14% for SNR_{diff}, 193% for SNR_{mean}, and 119% for SNR_{stdv}.

The SNR ratios for different acquisition techniques and reconstruction filters are shown in Table 1. Significant differences in comparison to SNR_{mult} are found for
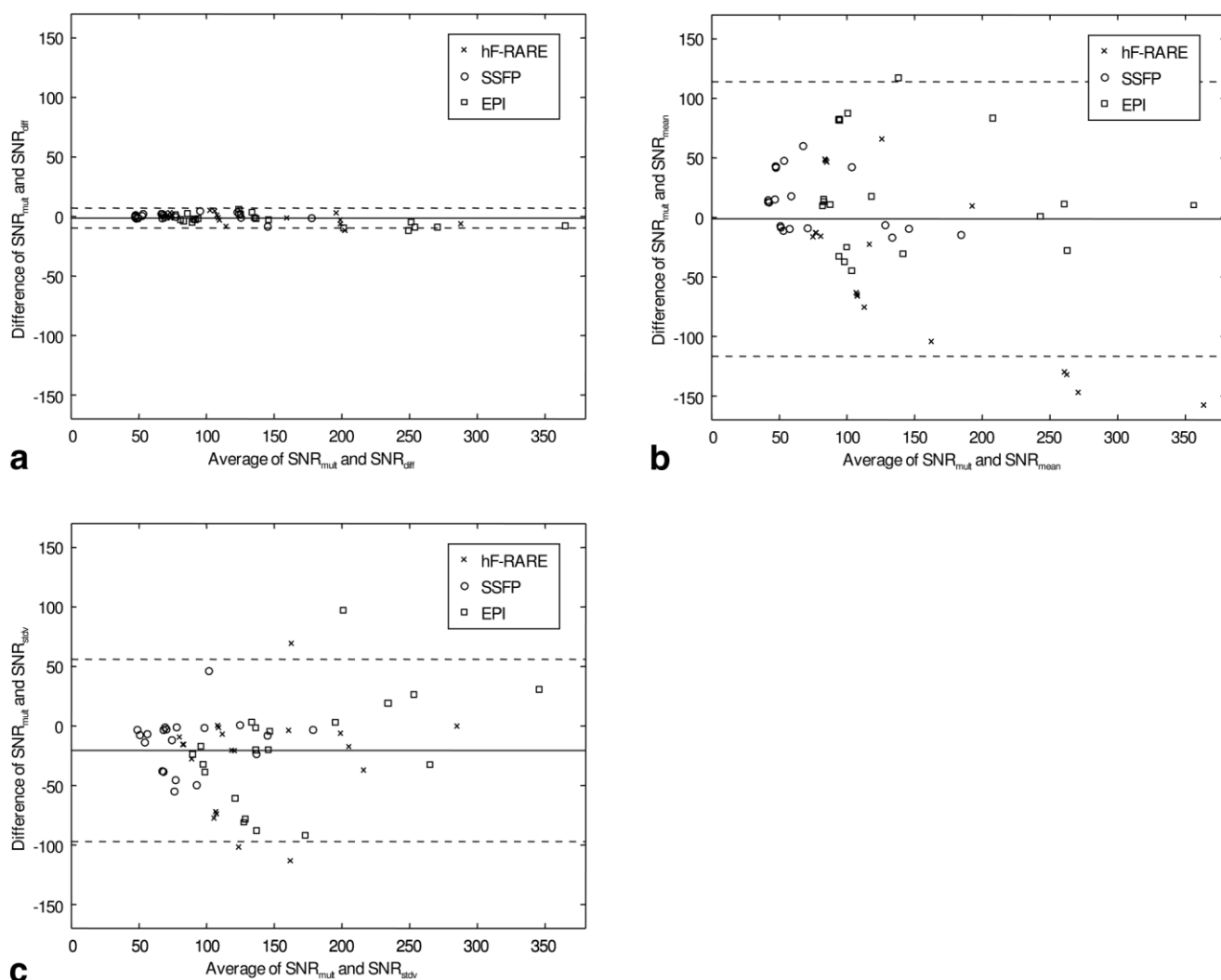

Figure 1. Bland-Altman plots showing the agreement between SNR_{mult} (the standard of reference) and SNR_{diff} (**a**), SNR_{mean} (**b**), and SNR_{stdv} (**c**) for the phantom measurements. Data for all sequences, acquisition techniques, and reconstruction filters are combined. Note that SNR_{diff} agrees much better with SNR_{mult} than SNR_{mean} and SNR_{stdv}.

Table 1
SNR Ratios (and SD) of Different Acquisition Techniques and Reconstruction Filters in Phantom Measurements*

SNR ratio	SNR ratio based on (%)			
	SNR_{mult} (SD)	SNR_{diff} (SD)	SNR_{mean} (SD)	SNR_{stdv} (SD)
Acquisition technique				
SNR(8CH)/SNR(1CH)	54.9 (0.5)	**53.8** (1.6)	**22.4** (5.2)	**62.5** (13.2)
SNR(GRAPPA)/SNR(nonaccelerated)	66.9 (2.9)	67.1 (4.7)	**138.3** (4.3)	**123.9** (8.6)
SNR(mSENSE)/SNR(nonaccelerated)	66.0 (4.5)	66.4 (5.7)	**218.5** (15.4)	**76.9** (4.5)
Reconstruction filter				
SNR(Hanning)/SNR(none)	146.4 (7.1)	145.7 (11.6)	145.8 (6.3)	142.0 (6.9)
SNR(Large FOV)/SNR(none)	101.1 (2.6)	101.4 (4.7)	**105.5** (3.4)	**116.1** (4.6)
SNR(Normalization)/SNR(none)	100.7 (2.6)	100.4 (5.4)	92.3 (18.4)	91.2 (17.7)
SNR(Elliptical)/SNR(none)	107.1 (5.3)	106.9 (6.6)	106.4 (6.5)	107.8 (7.8)

*Significant differences ($P < 0.05$) in comparison to SNR_{mult} ratios are in bold.

SNR_{mean} and SNR_{stdv}, and in one case for SNR_{diff}. For example, when GRAPPA or mSENSE were applied, the SNR decreased to about 67% of its original value without parallel imaging. However, based on SNR_{mean}, an apparent increase of the SNR to 138% and 219% was found. Based on SNR_{stdv}, the SNR appears increased for GRAPPA and decreased for mSENSE, but only to 77% of its original value. When reconstruction filters are applied, significant differences are found for the large-FOV filter: SNR_{mult} and SNR_{diff} are unchanged, while SNR_{mean} and SNR_{stdv} appear to increase to 106% and 116%, respectively.

Based on the pixel-by-pixel SD determined for SNR_{mult}, the spatial distribution of noise for different phantom experiments is shown in Fig. 2. The noise is homogeneously distributed in acquisitions without parallel imaging with no filter, the Hanning filter, or the elliptical reconstruction filter. Spatially varying noise levels are found in acquisitions applying either parallel imaging or the large-FOV or intensity-normalization filter.

In Vivo Measurements

For the measurements in vivo, the deviations from the reference measurement, SNR_{diff}, range from 0.8% to 66.1% for SNR_{mean} and from 0.1% to 40.8% for SNR_{stdv}. Averaged over all measurements, the deviations from SNR_{diff} are 30.1% ($\pm$ SD 23.6%) for SNR_{mean} and 16.0% ($\pm$ 11.6%) for SNR_{stdv}.

The deviations of SNR_{mean} were greater than 10% in 13 of 20 measurements. These include all measurements with the 8CH coil without parallel imaging, as well as with GRAPPA. The deviation was lower than 10% only in the nonaccelerated 1CH acquisitions with no filter, the large-FOV filter, or the elliptical filter, and in all filtered mSENSE acquisitions.

The deviations of SNR_{stdv} were greater than 10% in 13 of 20 measurements as well. These include all GRAPPA measurements, all filtered 1CH measurements, the nonaccelerated 8CH measurement with no reconstruction filter, and the mSENSE measurements with no
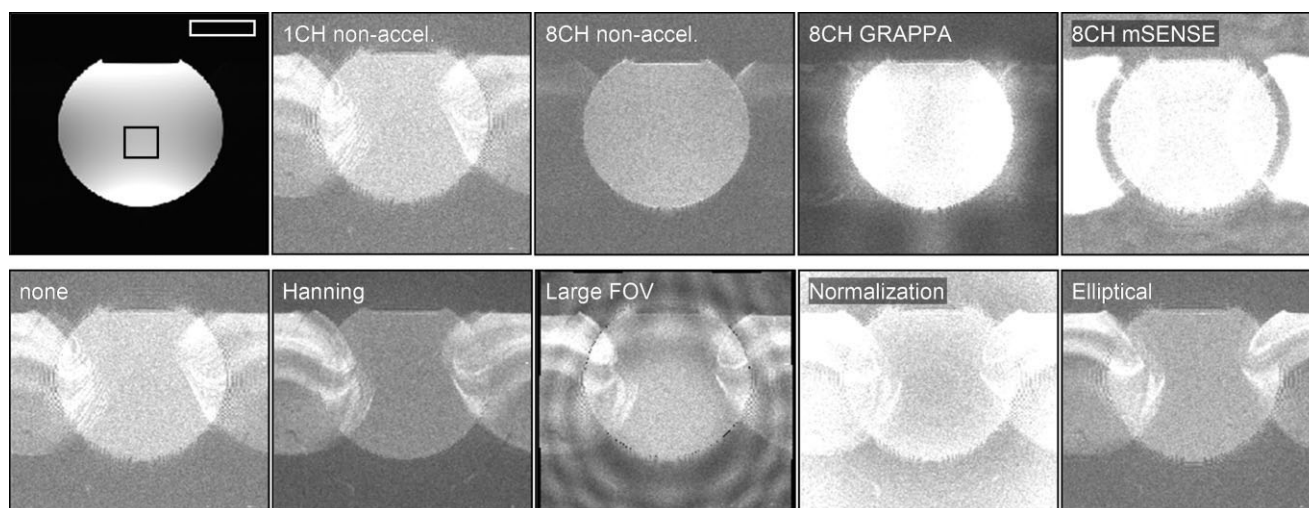

Figure 2. ROI positions and spatial noise distribution. The black ROI was used for SNR calculations with the methods SNR_{mult} and SNR_{diff}, and to calculate the mean signal intensity for SNR_{mean} and SNR_{stdv}. The white ROI was used to calculate the noise intensity for SNR_{mean} and SNR_{stdv}. The noise maps show the SD calculated pixel by pixel from 95 repetitions of an identical acquisition for different acquisition techniques without a reconstruction filter (top row) and for different reconstruction filters based on data of the 1CH head coil acquisitions (bottom row).
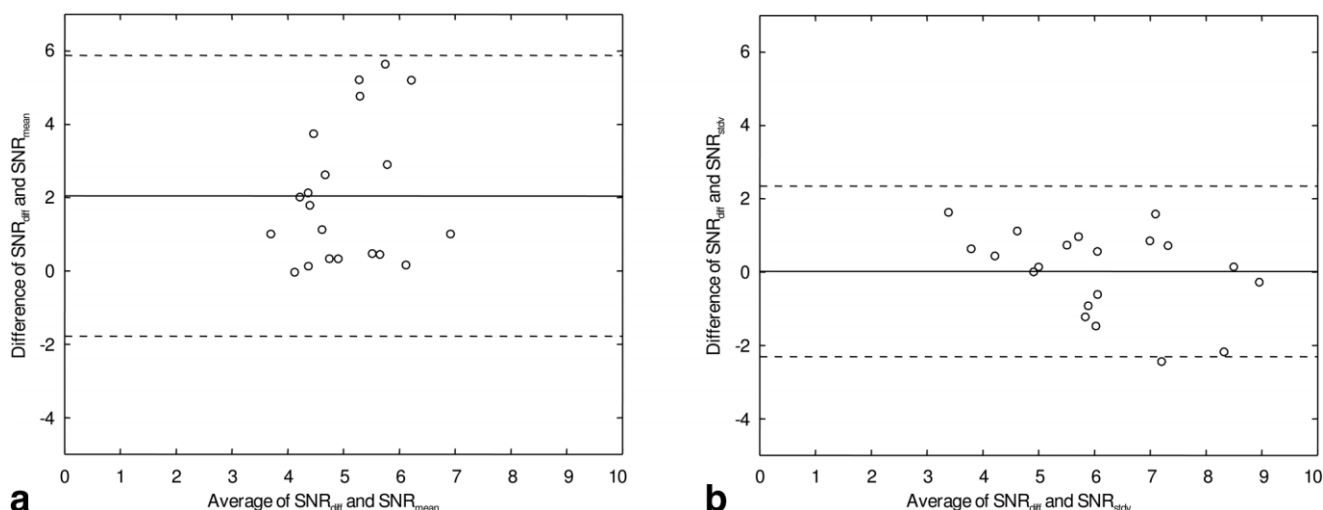
Figure 3. Bland-Altman plots showing the agreement between SNR_{diff} (the standard of reference) and SNR_{mean} (**a**) and SNR_{stdv} (**b**) for the measurements in vivo. Data for all acquisition techniques and reconstruction filters are combined.

filter, with the Hanning filter, and with the intensity-normalization filter.

The deviations of SNR_{mean} and SNR_{stdv} from SNR_{diff} are presented as Bland-Altman plots in Fig. 3, which shows 95%-CIs between –1.8 and 5.9 for SNR_{mean} and between –2.3 and 2.3 for SNR_{stdv}. The ratio of the range of the 95%-CI and the average SNR is 152% for SNR_{mean}, and 77% for SNR_{stdv}.

Comparing the SNR ratios for different acquisition techniques and different reconstruction filters in Table 2, similar results as in the phantom experiments are found. For example, when applying GRAPPA or mSENSE as the reference, SNR_{diff}, is decreased to about 75% and 61% of its original value without parallel imaging. However, based on SNR_{mean}, an apparent increase of the SNR to 121% and 150% is found, and based on SNR_{stdv} the SNR appears unchanged for GRAPPA and decreased for mSENSE to 55% of its original value.

The subtraction images used to calculate SNR_{diff} are displayed in Fig. 4. They do not show enhanced edge contrast in the area of the liver where the ROI was positioned. Artifacts due to slight misregistrations are visible around the central large vessels, the left lung, and the stomach.

DISCUSSION

The results presented above demonstrate that, in general, the SNR measured by the two-region approaches SNR_{mean} or SNR_{stdv} will not agree with the actual SNR as measured by SNR_{mult} and SNR_{diff}. This is particularly true after the application of reconstruction filters, such as an intensity-normalization filter or large-FOV filter, after multichannel reconstruction, or after parallel imaging.

For the phantom measurements, the calculated deviations of the three examined methods of SNR measurement from the reference method SNR_{mult} show that only the difference method provides accurate results in all measurements with deviations below 10%. In contrast, both two-region approaches do not accurately determine the SNR of the acquisitions in most cases, with deviations up to 140%. This is also demonstrated by the Bland-Altman plots with 95%-CIs that are comparable in width to the actual SNR values for SNR_{mean} and SNR_{stdv}. To explain these findings, both the statistical noise distribution and the spatial homogeneity of the noise must be considered.

The statistical noise distribution describes the intensity distribution of the image signal in the presence of

Table 2
SNR Ratios (and SD) of Different Acquisition Techniques and Reconstruction Filters in Measurements In Vivo

| SNR ratio	SNR ratio based on (%)		
	SNR_{diff} (SD)	SNR_{mean} (SD)	SNR_{stdv} (SD)
Acquisition technique			
SNR(8CH)/SNR(1CH)	135.3 (16.3)	57.2 (3.9)	135.3 (5.5)
SNR(GRAPPA)/SNR(non-accel.)	74.5 (7.8)	120.6 (8.7)	102.8 (9.3)
SNR(mSENSE)/SNR(non-accel.)	60.7 (6.8)	150.1 (18.5)	54.8 (7.9)
Reconstruction filter			
SNR(Hanning)/SNR(none)	136.0 (16.7)	148.6 (27.0)	156.8 (31.7)
SNR(Large FOV)/SNR(none)	113.4 (3.5)	117.2 (17.7)	146.1 (30.0)
SNR(Normalization)/SNR(none)	95.4 (10.2)	105.3 (18.9)	103.5 (23.1)
SNR(Elliptical)/SNR(none)	105.7 (7.7)	115.3 (13.9)	117.2 (26.0)
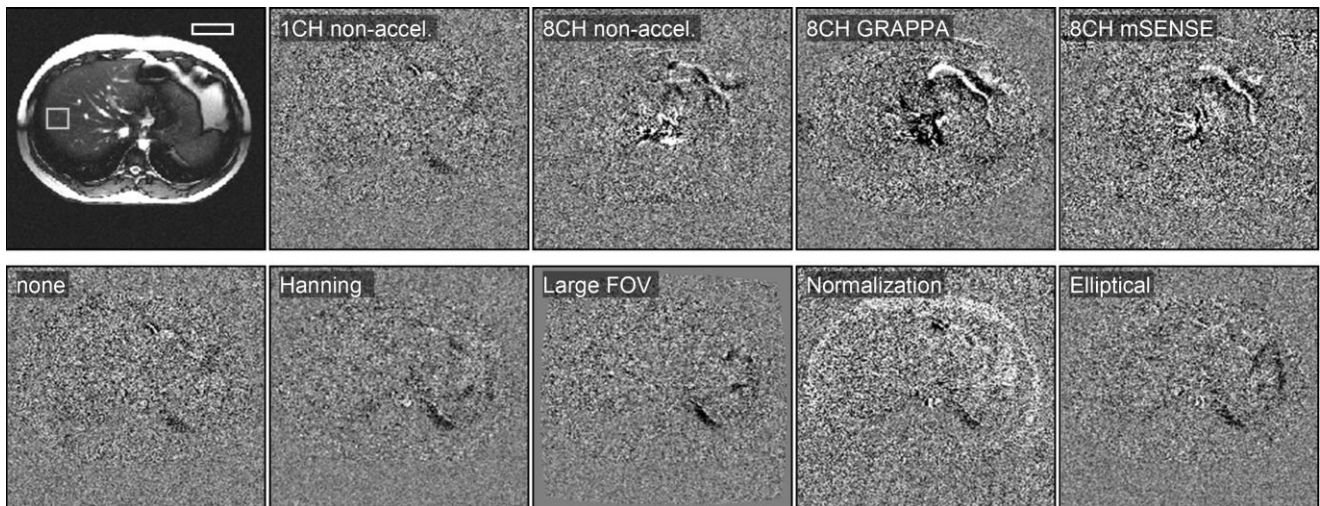
Figure 4. ROI positions and difference images. The square ROI was used for SNR calculations with the methods SNR_{mult} and SNR_{diff}, and to calculate the mean signal intensity for SNR_{mean} and SNR_{stdv}. The rectangular ROI was used to calculate the noise intensity for SNR_{mean} and SNR_{stdv}. The difference images are calculated from two repetitions of identical acquisitions for different acquisition techniques (top row) and different reconstruction filters (bottom row).

noise, i.e., the probability of finding a certain deviation from the true signal that would be observed without noise. The original noise in the image raw data prior to its reconstruction with Fourier transformation typically has a normal (or Gaussian) distribution (30). However, this statistical distribution changes during image reconstruction. In the case of reconstructing data from a single receiver channel using the Fourier transform and subsequent magnitude calculation, the background signal of the calculated image is described by the Rayleigh distribution (31). The correction factors used for the determination of SNR_{mean} or SNR_{stdv} (1,2) are based on the properties of this distribution. Therefore, SNR_{mean} or SNR_{stdv} can only be expected to be valid methods of SNR calculation if the noise in the image background follows the Rayleigh distribution statistics. In our measurements, this should be the case for 1CH acquisitions with the SSFP and EPI sequence, where the deviations of SNR_{mean} or SNR_{stdv} were less than 10%. The 1CH acquisitions of the hF-RARE sequence have a different noise distribution since they were reconstructed as a real-part image, and negative data were removed by magnitude calculation afterwards. This special reconstruction is based on the Margosian algorithm for half-Fourier data (32).

The 8CH acquisitions without parallel imaging were reconstructed using the SoS method (6,33), resulting in a noncentral chi-distribution (7) of the signal. This distribution differs considerably from the Rayleigh distribution; in particular, the mean value of the background noise is substantially increased. Thus, SNR_{stdv} and especially SNR_{mean} will fail to determine the true SNR. Similarly, in 8CH acquisitions with the parallel-imaging algorithms GRAPPA or mSENSE, the noise distribution must be expected to differ from the Rayleigh distribution.

SNR_{stdv} and in particular SNR_{mean} will be considerably biased if the noise intensities are not described by a Rayleigh distribution. Therefore, it is important to verify that the background noise has a Rayleigh distribution before determining SNR_{stdv} or SNR_{mean}. This can be done by calculating the ratio of the mean value and the SD of the background noise. If this ratio differs significantly from 1.91, the background noise is not described by a Rayleigh distribution and the two-region approaches should not be used (2).

In addition to a modified statistical noise distribution, the SNR determination in parallel imaging is influenced by the inhomogeneous spatial distribution of noise described by the *g*-factor. Depending on the coil geometry, the noise can be increased or decreased in background regions (Fig. 2), and the SNR may appear lower or higher depending on the positioning of the background ROI when using the two-region approach. This effect can increase, decrease, or accidentally compensate for the SNR bias due to a modified statistical distribution of noise.

Inhomogeneously distributed noise intensities also cause deviations of the SNRs with different reconstruction filters. In particular, the intensity-normalization filter adds a spatially varying scaling to the image data that influences SNR calculations if different ROIs are used for signal and noise measurements. In the case of the 1CH acquisition, this means that the image intensity in the center is reduced (Fig. 2), resulting in an apparently decreased SNR when using a two-region approach. The large-FOV filter works by spatially distorting image areas close to the edges of the FOV. Since the noise intensity is measured in those areas, SNR_{mean} and SNR_{stdv} are influenced by this filter as well. In contrast, the Hanning and elliptical filters do not affect the accuracy of the SNR measurements with the two-region approach. When these filters are applied, the noise remains homogeneously distributed over the complete image.

It is important to distinguish two different consequences of the observed SNR deviations. The first one is the bias of the determined absolute SNR; however, if

this bias can be described by a constant factor for several measurements, the relative change of the SNR may be determined correctly. For example, calculating SNR_{mean} or SNR_{stdv} for a conventional and unfiltered 1CH acquisition as suggested in Ref. (1) *without* the appropriate scaling factors given in Eqs. [A11] and [A12] of Appendix A will result in systematically biased SNR measurements because of the Rayleigh noise distribution. Nevertheless, SNR comparisons for different tissues or pulse sequences remain valid because the constant factor will cancel when calculating any relative SNR change.

However, a second, more problematic consequence must be considered when using the two-region approach to compare different acquisition techniques or reconstructions with different filters, as in Table 1. In this case the SNR deviation will in general be different for each acquisition, and hence the SNR change cannot be calculated correctly. This is illustrated by our 8CH measurements without parallel imaging, with GRAPPA, and with mSENSE. An SNR decrease due to parallel imaging is to be expected in agreement with the theory providing that $SNR_R = SNR_0/(g\sqrt{R})$ for a geometry factor g (always ≥ 1) and an acceleration factor R (4). For parallel imaging with an acceleration factor of $R = 2$, this results in a minimum decrease to $1/\sqrt{2} \approx 70.7\%$ of the original SNR. While SNR_{mult} and SNR_{diff} demonstrate this expected reduction of the SNR, the opposite is found when comparing SNR_{mean} or SNR_{stdv} in nonaccelerated acquisitions and with GRAPPA: the SNR appears paradoxically *increased* with parallel imaging! Analogously, SNR_{mean} is apparently increased when applying mSENSE, while SNR_{stdv} is decreased but to a smaller extent than the reference SNR. This may explain the "somewhat puzzling" g-factor < 1 reported in Ref. 12.

Our measurements in vivo confirm the results of the phantom measurements. As described above, we used SNR_{diff} instead of SNR_{mult} as the standard of reference in vivo. Apart from practical reasons, this decision was also justified by the results of the phantom measurements, which showed a mean difference of only 2.7% between both methods.

The measured values of SNR_{diff} show a very similar behavior as in the phantom measurements when comparing 8CH acquisitions without and with parallel imaging, or acquisitions without reconstruction filter and with the Hanning or elliptical filter (Table 2). Applying parallel imaging, SNR_{diff} is substantially decreased, and applying the Hanning or elliptical reconstruction filters, an increased SNR_{diff} is observed. This agreement with the phantom measurements indicates that SNR_{diff} is a valid method to calculate the SNR. In contrast to the phantom measurements, the reference SNR is increased when switching from the conventional 1CH body coil to the 8CH coil. This can be explained by the improved fill factor of the latter.

In general, the measurements in vivo must be expected to be less precise because of the lower reproducibility of each acquisition. Since the calculation of SNR_{diff} is based on a difference image, any remaining respiratory motion or blood flow causes artifacts in the subtraction image, which increases the apparent noise intensity. Nevertheless, the images in Fig. 4 demonstrate that these artifacts remained at low levels in our measurements. The lower reproducibility in subsequent acquisitions, however, is another reason why SNR_{mult} was not measured in vivo, since involuntary patient motion would result in accumulated errors over time and increase the calculated SD (i.e., the apparent noise level).

One of the most important results of the in vivo experiments is the substantial deviation of SNR_{mean} and SNR_{stdv} from the reference SNR, especially for the 8CH coil without parallel imaging or with GRAPPA. As in the phantom measurements, SNR_{mean} is paradoxically increased when using GRAPPA or mSENSE, and SNR_{stdv} does not show the true SNR decrease either (Table 2). Therefore, both the phantom measurements and the measurements in vivo indicate that the two-region approaches SNR_{mean} and SNR_{stdv} should not be used for SNR determinations in most situations, i.e., in acquisitions using multichannel phased-array coils, reconstruction filters, or parallel imaging.

In conclusion, our results demonstrate that the SNR measured by evaluating a foreground and a background region will in general not agree with the true SNR, particularly after the application of certain reconstruction filters, multichannel reconstruction, or parallel imaging. Consequently, paradoxical results, such as an apparent increase of SNR with parallel imaging compared to nonaccelerated imaging with identical acquisition parameters, may be observed. This result may have important implications for future comparisons of different conventional and parallel-imaging reconstruction methods used for various clinical and methodological studies.

In general, before applying one of the two-region approaches (SNR_{mean}/SNR_{stdv}), one must verify whether the two following conditions are fulfilled:

1. The statistical intensity distribution of the background noise must be a Rayleigh distribution. This is the case for magnitude images calculated from a single set of complex raw data.

2. The spatial distribution of noise must be homogeneous. This is the case after a conventional standard reconstruction (Fourier transform); however, the application of certain reconstruction filters or newer imaging techniques, such as parallel imaging or complex iterative image reconstruction methods, typically results in an inhomogeneous noise distribution.

Only if these two conditions are fulfilled will the two-region approaches be valid. It is generally recommended to calculate SNR_{stdv} rather than SNR_{mean} because the SD of noise is less variable than its mean value (7).

However, with the increasing complexity of MRI systems providing multiple channels and complicated reconstruction algorithms, the number of measurements that fulfill both conditions is decreasing. As soon as reconstruction filters or techniques such as parallel imaging influence the spatial noise distribution, only those methods of SNR measurement remain valid that determine the noise at the same spatial position as the signal. These are the SNR_{diff}, SNR_{NEMA}, SNR_{units}, and SNR_{mult} methods. Since the SNR_{units} and SNR_{NEMA} meth-

ods require special acquisition and reconstruction techniques, and the SNR_{mult} method is based on the acquisition of a relatively large number of identical acquisitions, only the SNR_{diff} method appears feasible for SNR measurements in clinical applications. It should be noted that the SNR_{units} and SNR_{NEMA} methods (21) are substantially more robust than the calculation of SNR_{diff}, and it would therefore be highly desirable that MRI system manufacturers provide support for these methods in future system generations. SNR_{mult} should be considered as an alternative if pixel-by-pixel measurements (of phantom images) are necessary.

APPENDIX A

Definition of SNR and Methods of SNR Determination

An idealized description of the image signal intensity S_N in the presence of noise in a series of K repeated acquisitions is given by

$$S_N(\mathbf{r},k) = S(\mathbf{r}) + N(\mathbf{r},k), \quad \text{(A1)}$$

where $S(\mathbf{r})$ is the "true" image intensity and $N(\mathbf{r}, k)$ is the superimposed noise in repetition $k = 1,...,K$ and at position $\mathbf{r} = (x, y, z)$. For simplicity, we will assume that $N(\mathbf{r}, k)$ is normally distributed in space (i.e., with respect to $\mathbf{r}$) and time (i.e., with respect to k) and is described by its mean value 0 and its SD σ. (This description of $S_N(\mathbf{r}, k)$ is valid only for sufficiently large SNRs, i.e., $S(\mathbf{r}) >> \sigma$; otherwise, more complicated distributions, such as the Rician (2,34–36) or noncentral chi distribution (7), have to be used for $S_N(\mathbf{r}, k)$.)

The SNR of a single image voxel at position $\mathbf{r} = (x, y, z)$ can now be defined as

$$SNR(\mathbf{r}) = \frac{S(\mathbf{r})}{\sigma}. \quad \text{(A2)}$$

To determine the SNR, two statistical measurements (one of the signal intensity S, and one of the original SD σ describing the noise) are required. While the signal intensity can be calculated as the mean value of the signal over all voxels of the ROI and/or all repetitions (the functions mean( ) and stddev( ) return the mean value and the SD of their arguments with respect to the variables and limits below them)

$$S(\mathbf{r}) = \underset{k=1...K}{\text{mean}}(S_N(\mathbf{r},k)) = m_K(\mathbf{r}) \quad \text{(A3a)}$$

$$S(\text{ROI},k) = \underset{\mathbf{r} \in \text{ROI}}{\text{mean}}(S_N(\mathbf{r},k)) = m_{\text{ROI}}(k) \quad \text{(A3b)}$$

$$S(\text{ROI}) = \underset{\substack{k=1...K \\ \mathbf{r} \in \text{ROI}}}{\text{mean}}(S_N(\mathbf{r},k)) = m_{\text{ROI},K} \quad \text{(A3c)}$$

(m as in m_K, m_{ROI}, or $m_{ROI,K}$ is used as an abbreviation for a mean value), the determination of σ is more difficult. The most straightforward method to calculate σ is based on the variation of the signal time course in repeated "identical" acquisitions (5,7,22–25):

$$\sigma(\mathbf{r}) = \underset{k=1...K}{\text{stddev}}(S_N(\mathbf{r},k)) = \underset{k=1...K}{\text{stddev}}(N(\mathbf{r},k)) = s_K(\mathbf{r}) \quad \text{(A4)}$$

(The s in s_K is used as an abbreviation for SD.) Now the SNR can be calculated as

$$SNR_{mult}(\mathbf{r}) = \frac{S_{mult}(\mathbf{r})}{\sigma_{mult}(\mathbf{r})} = \frac{\underset{k=1...K}{\text{mean}}(S_N(\mathbf{r},k))}{\underset{k=1...K}{\text{stddev}}(S_N(\mathbf{r},k))} = \frac{m_K(\mathbf{r})}{s_K(\mathbf{r})}, \quad \text{(A5)}$$

i.e., as the mean value of the pixel signal with respect to the time series divided by the SD of the pixel signal with respect to the time series (the index "mult" denotes that multiple acquisitions are required to determine the SNR). The SNR of an ROI is given by

$$SNR_{mult} = \frac{S_{mult}}{\sigma_{mult}} = \frac{\underset{\mathbf{r} \in \text{ROI}}{\text{mean}}(m_K(\mathbf{r}))}{\underset{\mathbf{r} \in \text{ROI}}{\text{mean}}(s_K(\mathbf{r}))} = \frac{\underset{\substack{\mathbf{r} \in \text{ROI} \\ k=1...K}}{\text{mean}}(S_N(\mathbf{r},k))}{\underset{\substack{\mathbf{r} \in \text{ROI} \quad k=1...K}}{\text{mean}}(\text{stddev}(S_N(\mathbf{r},k)))}$$

$$= \frac{m_{\text{ROI},K}}{m_{s_K(\mathbf{r})}} \quad \text{(A6)}$$

assuming that the spatial variation of $s_K(\mathbf{r})$ can be neglected within the ROI. The SNR_{mult} in an ROI is determined as the quotient of the mean value of the signal (this mean value can be calculated with respect to all pixels in the ROI and to all repetitions) and the mean value of the temporal SD of the signal (i.e., first the SD of the signal with respect to the repetitions is calculated for each pixel in the ROI and then averaged within the ROI).

Since repeated acquisitions are time-consuming and may be influenced by systematic signal variations due to patient motion or physiological signal variations, simpler methods requiring fewer acquisitions are typically applied for SNR measurements. Using only two acquisitions k_1 and k_2, the average SNR in an ROI can be determined as (19–22):

$$SNR_{diff}(k_1,k_2) = \frac{S_{diff}}{\sigma_{diff}} = \frac{\frac{1}{2}\underset{\mathbf{r} \in \text{ROI}}{\text{mean}}(S_N(\mathbf{r},k_1) + S_N(\mathbf{r},k_2))}{\frac{1}{\sqrt{2}}\underset{\mathbf{r} \in \text{ROI}}{\text{stddev}}(S_N(\mathbf{r},k_1) - S_N(\mathbf{r},k_2))}$$

$$= \frac{\frac{1}{2}m_{sum}}{\frac{1}{\sqrt{2}}s_{diff}} = \frac{1}{\sqrt{2}}\frac{m_{sum}}{s_{diff}}. \quad \text{(A7)}$$

The SNR_{diff} in an ROI is calculated as the quotient of the mean value (with respect to the ROI) of the signal in the sum image and the SD (evaluated in the same ROI) of the signal in the difference image, divided by the factor $\sqrt{2}$. Since Eq. [A7] is based on the assumption of a Gaussian noise distribution within the ROI in the difference image, this ROI must be positioned in tissue with sufficiently high SNR (and *not* in the image background).

A second technique suggested in the NEMA standard MS 1-2001 (21) is based on the acquisition of a normal image and a pure noise image. The signal S_{NEMA} is calculated as mean value of the normal acquisition m_{img}, and the noise σ_{NEMA} from the SD of the noise image s_{noise} multiplied by $\sqrt{\frac{2}{4-\pi}}$ assuming a Rayleigh distribution and using an ROI at the same position as in the normal image:

$$SNR_{NEMA}(img,noise) = \frac{S_{NEMA}}{\sigma_{NEMA}}$$

$$= \frac{\underset{r \in ROI_{tissue}}{mean}(S_N(r,img))}{\sqrt{\frac{2}{4-\pi}}\underset{r \in ROI_{tissue}}{stddev}(S_N(r,noise))} = \frac{m_{img}}{\sqrt{\frac{2}{4-\pi}}s_{noise}}. \quad (A8)$$

A disadvantage of this method is that most MRI systems do not permit the acquisition of a pure noise scan with standard pulse sequences. This is especially demanding when using parallel-imaging techniques with integrated reference scans, such as GRAPPA, since the noise data must be reconstructed using the same coil sensitivity profiles that have been acquired for the image itself.

If images are reconstructed in "SNR units," as suggested by Kellman and McVeigh (23), SNR determination becomes trivial, since the pixel intensities directly represent the SNR, and thus the SNR can be determined for a single pixel or an ROI simply by measuring the pixel intensity

$$SNR_{units}(r) = S_{units}(r). \quad (A9)$$

or the mean intensity of an ROI

$$SNR_{units} = S_{units} = \underset{r \in ROI}{mean}(S_{units}(r)) = m_{ROI} \quad (A10)$$

While SNR determination is very simple for images in SNR units, the reconstruction of these images is complicated and requires severe modifications of pulse sequences and reconstruction algorithms, as mentioned above.

Finally, the techniques most often used to determine the SNR are those that are based on the signal statistics in two separate ROIs of a single image k: one in the tissue of interest (ROI_{tissue}), and one in the image background (ROI_{air}) (1,2). The SNR is calculated as

$$SNR_{mean}(k) = \frac{S_{mean}}{\sigma_{mean}} = \frac{\underset{r \in ROI_{tissue}}{mean}(S_N(r,k))}{\sqrt{\frac{2}{\pi}}\underset{r \in ROI_{air}}{mean}(S_N(r,k))} = \frac{m_{tissue}}{\sqrt{\frac{2}{\pi}}m_{air}} \quad (A11)$$

or

$$SNR_{stdv}(k) = \frac{S_{mean}}{\sigma_{stdv}} = \frac{\underset{r \in ROI_{tissue}}{mean}(S_N(r,k))}{\sqrt{\frac{2}{4-\pi}}\underset{r \in ROI_{air}}{stddev}(S_N(r,k))} = \frac{m_{tissue}}{\sqrt{\frac{2}{4-\pi}}s_{air}} \quad (A12)$$

using either the mean value or the SD of the background signal. The correction factors $\sqrt{\frac{2}{4-\pi}} \approx 1.53$ and $\sqrt{\frac{2}{\pi}} \approx 0.80$ in Eqs. [A11] and [A12] are required because of the Rayleigh distribution of background noise in magnitude images (31).

REFERENCES

1. Kaufman L, Kramer DM, Crooks LE, Ortendahl DA. Measuring signal-to-noise ratios in MR imaging. Radiology 1989;173:265–267.
2. Henkelman RM. Measurement of signal intensities in the presence of noise in MR images. Med Phys 1985;12:232–233.
3. Sodickson DK, Manning WJ. Simultaneous acquisition of spatial harmonics (SMASH): fast imaging with radiofrequency coil arrays. Magn Reson Med 1997;38:591–603.
4. Pruessmann KP, Weiger M, Scheidegger MB, Boesiger P. SENSE: sensitivity encoding for fast MRI. Magn Reson Med 1999;42:952–962.
5. Sodickson DK, Griswold MA, Jakob PM, Edelman RR, Manning WJ. Signal-to-noise ratio and signal-to-noise efficiency in SMASH imaging. Magn Reson Med 1999;41:1009–1022.
6. Roemer PB, Edelstein WA, Hayes CE, Souza SP, Mueller OM. The NMR phased array. Magn Reson Med 1990;16:192–225.
7. Constantinides CD, Atalar E, McVeigh ER. Signal-to-noise measurements in magnitude images from NMR phased arrays. Magn Reson Med 1997;38:852–857 (Erratum in: Magn Reson Med 2004; 52:219).
8. Hagspiel KD, Yao L, Shih MC, Burkholder B, Bissonette E, Harthun NL. Comparison of multistation MR angiography with integrated parallel acquisition technique versus conventional technique with a dedicated phased-array coil system in peripheral vascular disease. J Vasc Interv Radiol 2006;17:263–269.
9. Vogt FM, Antoch G, Hunold P, et al. Parallel acquisition techniques for accelerated volumetric interpolated breath-hold examination magnetic resonance imaging of the upper abdomen: assessment of image quality and lesion conspicuity. J Magn Reson Imaging 2005; 21:376–382.
10. Kuhl CK, Gieseke J, von Falkenhausen M, et al. Sensitivity encoding for diffusion-weighted MR imaging at 3.0 T: intraindividual comparative study. Radiology 2005;234:517–526.
11. de Vries M, Nijenhuis RJ, Hoogeveen RM, et al. Contrast-enhanced peripheral MR angiography using SENSE in multiple stations: feasibility study. J Magn Reson Imaging 2005;21:37–45.
12. Chen Q, Quijano CV, Mai VM, et al. On improving temporal and spatial resolution of 3D contrast-enhanced body MR angiography with parallel imaging. Radiology 2004;231:893–899.
13. Fink C, Puderbach M, Bock M, et al. Regional lung perfusion: assessment with partially parallel three-dimensional MR imaging. Radiology 2004;231:175–184.
14. Ruel L, Brugieres P, Luciani A, Breil S, Mathieu D, Rahmouni A. Comparison of in vitro and in vivo MRI of the spine using parallel imaging. AJR Am J Roentgenol 2004;182:749–755.
15. Hunold P, Maderwald S, Ladd ME, Jellus V, Barkhausen J. Parallel acquisition techniques in cardiac cine magnetic resonance imaging using TrueFISP sequences: comparison of image quality and artifacts. J Magn Reson Imaging 2004;20:506–511.
16. Yoshioka H, Sato J, Takahashi N, et al. Dual double arterial phase dynamic MR imaging with sensitivity encoding (SENSE): which is better for diagnosing hypervascular hepatocellular carcinomas, in-phase or opposed-phase imaging? Magn Reson Imaging 2004;22: 361–367.
17. Quick HH, Vogt FM, Maderwald S, et al. High spatial resolution whole-body MR angiography featuring parallel imaging: initial experience. Rofo Fortschr Geb Rontgenstr Neuen Bildgeb Verfahr 2004;176:163–169.
18. Willinek WA, Gieseke J, von Falkenhausen M, Neuen B, Schild HH, Kuhl CK. Sensitivity encoding for fast MR imaging of the brain in patients with stroke. Radiology 2003;228:669–675.
19. Murphy BW, Carson PL, Ellis JH, Zhang YT, Hyde RJ, Chenevert TL. Signal-to-noise measures for magnetic resonance imagers. Magn Reson Imaging 1993;11:425–428.

20. Firbank MJ, Coulthard A, Harrison RM, Williams ED. A comparison of two methods for measuring the signal to noise ratio on MR images. Phys Med Biol 1999;44:N261–N264.

21. National Electrical Manufacturers Association (NEMA). Determination of signal-to-noise ratio (SNR) in diagnostic magnetic resonance imaging. NEMA Standards Publication MS 1-2001. Rosslyn: National Electrical Manufacturers Association; 2001. 15 p.

22. Reeder SB, Wintersperger BJ, Dietrich O, et al. Practical approaches to the evaluation of signal-to-noise ratio performance with parallel imaging: application with cardiac imaging and a 32-channel cardiac coil. Magn Reson Med 2005;54:748–754.

23. Kellman P, McVeigh ER. Image reconstruction in SNR units: a general method for SNR measurement. Magn Reson Med 2005;54: 1439–1447.

24. Griswold MA, Jakob PM, Chen Q, et al. Resolution enhancement in single-shot imaging using simultaneous acquisition of spatial harmonics (SMASH). Magn Reson Med 1999;41:1236–1245.

25. Bodurka J, Ledden PJ, van Gelderen P, et al. Scalable multichannel MRI data acquisition system. Magn Reson Med 2004;51:165–171.

26. Griswold MA, Jakob PM, Heidemann RM, et al. Generalized autocalibrating partially parallel acquisitions (GRAPPA). Magn Reson Med 2002;47:1202–1210.

27. Griswold MA, Kannengiesser S, Heidemann RM, Wang J, Jakob PM. Field-of-view limitations in parallel imaging. Magn Reson Med 2004;52:1118–1126.

28. Bland JM, Altman DG. Statistical methods for assessing agreement between two methods of clinical measurement. Lancet 1986;1:307–310.

29. Bland JM, Altman DG. Comparing methods of measurement: why plotting difference against standard method is misleading. Lancet 1995;346:1085–1087.

30. McVeigh ER, Henkelman RM, Bronskill MJ. Noise and filtration in magnetic resonance imaging. Med Phys 1985;12:586–591.

31. Edelstein WA, Bottomley PA, Pfeifer LM. A signal-to-noise calibration procedure for NMR imaging systems. Med Phys 1984;11:180–185.

32. Margosian P, Schmitt F, Purdy D. Faster MR imaging: imaging with half the data. Health Care Instrum 1986;1:195–197.

33. Larsson EG, Erdogmus D, Yan R, Principe JC, Fitzsimmons JR. SNR-optimality of sum-of-squares reconstruction for phased-array magnetic resonance imaging. J Magn Reson 2003;163:121–123.

34. Rice SO. Mathematical analysis of random noise. In: Wax N, editor. Selected papers on noise and stochastic processes. New York: Dover Publications; 1954. p 133–294.

35. Holden JE, Halama JR, Hasegawa BH. The propagation of stochastic pixel noise into magnitude and phase values in the Fourier analysis of digital images. Phys Med Biol 1986;31:383–396.

36. Gudbjartsson H, Patz S. The Rician distribution of noisy MRI data. Magn Reson Med 1995;34:910–914 (Erratum in: Magn Reson Med 1996;36:332).